USP28 deletion and small molecule inhibition destabilises c-Myc and elicits regression of squamous cell lung carcinoma

E. Josue Ruiz[1] , Adan Pinto-Fernandez[2], Andrew P. Turnbull[3], Linxiang Lan[1], Thomas M. Charlton[2], Hannah Claire Scott[2], Andreas Damianou[2], George Vere[2], Eva M. Riising[1], Clive Da Costa[1], Wojciech W. Krajewski[3], David Guerin[4,10], Jeffrey Kearns[4,11], Stephanos Ioannidis[4,12], Marie Katz[4,13], Jonathan C. O'Connell[4,13], Natalia Moncaut[1], Ian Rosewell[5], Emma Nye[1], Neil Jones[3], Claire Heride[3], Malte Gersch[6], Christopher J. Dinsmore[4,14], Tim R. Hammonds[3,15], Sunkyu Kim[16], David Komander[7], Sylvie Urbé[8], Michael J. Clague[9], Benedikt M. Kessler[2,17] and Axel Behrens[1,9,17]

[1] Adult stem cell laboratory; The Francis Crick Institute, 1 Midland Road, London NW1 1AT, UK
[2] Target Discovery Institute, Nuffield Department of Medicine, University of Oxford, Roosevelt Drive, Oxford OX3 7FZ, UK
[3] CRUK Therapeutic Discovery Laboratories, London Bioscience Innovation Centre, London NW1 0NH, UK
[4] FORMA Therapeutics, Arsenal Street, Watertown, Massachusetts 02472, USA
[5] Genetic Manipulation Service, The Francis Crick Institute, 1 Midland Road, London NW1 1AT, UK
[6] Max Planck Institute of Molecular Physiology, Otto-Hahn-Str 11, 44227 Dortmund, Germany
[7] The Walter and Eliza Hall Institute of Medical Research, 1G Royal Parade, Parkville 3052, VIC, Australia
[8] Cellular and Molecular Physiology, Institute of Translational Medicine, University of Liverpool, Crown Street, Liverpool L69 3BX, UK
[9] King's College London, Faculty of Life Sciences and Medicine, Guy's Campus, London SE1 1UL, UK
[10] Present address: Tango Therapeutics, 100 Binney Street, Cambridge, MA 02142, USA
[11] Present address: Novartis Institutes for BioMedical Research, 250 Massachusetts Ave, Cambridge, MA 02139, USA
[12] Present address: H3 Biomedicine, 300 Technology Square, Cambridge, MA 02139, USA
[13] Present address: Valo Health, 399 Boylston St, Suite 505, Boston, MA 02116, USA
[14] Present address: Third Rock Ventures, 29 Newbury Street, Boston, MA 02116, USA
[15] Present address: Loki Therapeutics, London Bioscience Innovation Centre, 2 Royal College Street, London NW1 0NH, UK
[16]Incyte, 1801 Augustine Cut-off, Wilmington, DE 19803, USA

[17]**Correspondence:**

Benedikt M Kessler	Axel Behrens
Target Discovery Institute	The Francis Crick Institute
University of Oxford	London
OX3 7FZ, UK	NW1 AT, UK
benedikt.kessler@ndm.ox.ac.uk	axel.behrens@crick.ac.uk

Running title: Essential function of USP28 in squamous cell lung cancer

Abstract (188 words)

Lung squamous cell carcinoma (LSCC) is a considerable global health burden, with an incidence of over 600,000 cases per year. Treatment options are limited, and patient 5-year survival rate is less than 5%. The ubiquitin specific protease 28 (USP28) has been implicated in tumorigenesis through its stabilization of the oncoprotein c-MYC. Here, we show that genetic inactivation of *USP28* induced regression of established murine LSCC lung tumors. We developed small molecule USP28 inhibitors that inhibit USP28 activity in the low nanomole range. While displaying considerable activity against the closest homologue USP25, these inhibitors showed a high degree of selectivity over other deubiquitinases. USP28 inhibitor treatment resulted in a dramatic decrease in c-Myc proteins levels and consequently induced substantial regression of autochthonous murine LSCC tumors and human LSCC xenografts, thereby phenocopying the effect observed by genetic deletion. Thus, USP28 may represent a promising therapeutic target for the treatment of squamous cell lung carcinoma.

Introduction

Lung cancer is the leading cause of cancer death worldwide. Based on histological criteria lung cancer can be subdivided into non-small cell lung cancer (NSCLC) and the rarer small cell lung cancer. The most common NSCLCs are lung adenocarcinoma (LADC) and squamous cell carcinoma (LSCC), with large cell carcinoma being less commonly observed. Progress has been made in the targeted treatment of LADC, largely due to the development of small-molecule inhibitors against EGFR, ALK, and ROS1 (Cardarella and Johnson, 2013). However, no targeted treatment options exist for LSCC patients (Hirsch et al., 2017; Novello et al., 2014). Consequently, despite having limited efficacy on LSCC patient survival, platinum-based chemotherapy remains the cornerstone of current LSCC treatment (Fennell et al., 2016; Isaka et al., 2017; Scagliotti et al., 2008). Therefore, there is an urgent need to identify novel druggable targets for LSCC treatment and to develop novel therapeutics.

The *FBXW7* protein product F-box/WD repeat-containing protein 7 (FBW7) is the substrate recognition component of an SCF-type ubiquitin ligase, which targets several well-known oncoproteins, including c-Myc, Notch, and c-Jun, for degradation (Davis et al., 2014). These oncoproteins accumulate in the absence of FBW7 function, and genetic analyses of human LSCC samples revealed common genomic alterations in *FBXW7* (Cancer Genome Atlas Research, 2012; Kan et al., 2010). In addition, FBW7 protein is undetectable by immunohistochemistry (IHC) in 69% of LSCC patient tumor samples (Ruiz et al., 2019). Genetically engineered mice harboring loss of *Fbxw7* concomitant with *KRasG12D* activation (KF mice) develop LSCC with 100% penetrance and short latency, as well as LADC (Ruiz et al., 2019). Thus, FBW7 is an important tumor suppressor in both human and murine lung cancer.

The deubiquitinase Usp28 opposes FBW7-mediated ubiquitination of the oncoproteins c-Myc and c-Jun, thereby stabilizing these proteins (Popov et al., 2007). In a murine model of colorectal cancer, deleting *Usp28* reduced size of established tumors and increased lifespan (Diefenbacher et al., 2014). Therefore, targeting USP28 in order to destabilize its substrates represents an attractive strategy to inhibit the function of c-Myc and other oncogenic transcription factors that are not amenable to conventional inhibition by small molecules.

Here, we describe the characterisation of a novel USP28 inhibitory compound (USP28i) and the genetic as well as chemical validation of USP28 as a promising therapeutic target for LSCC tumors. Using an FRT/FLP and CRE/LOXP dual recombinase system (Schonhuber et al., 2014), we show that *Usp28* inactivation in established LSCC results in dramatic tumor regression. Importantly, USP28i treatment recapitulates LSCC regression in both mouse models and human LSCC xenografts. Absence or inhibition of USP28 resulted in a dramatic decrease in the protein levels of c-Myc, providing a potential mechanism of action for USP28i. Therefore, USP28 inhibition should be a strong candidate for clinical evaluation, particularly given the paucity of currently available therapy options for LSCC patients.

Results

USP28 is required to maintain protein levels of c-Myc, c-Jun and Δp63 in LSCC

To gain insights into the molecular differences between LADC and LSCC, we investigated the expression of MYC in these common NSCLCs subtypes. MYC was transcriptionally upregulated in human LSCC compared to healthy lung tissue or LADC tumors (**Figure 1A**). Quantitative polymerase chain reaction (qPCR) analysis on an independent set of primary human lung biopsy samples confirmed that MYC is highly expressed in LSCC tumors compared with normal lung tissue (**Figure 1B**). Moreover, immunohistochemistry (IHC) staining on primary lung tumors confirmed a significant abundance of c-Myc protein in LSCC samples (**Figure 1C, 1D**). Consequenty, c-Myc downregulation by siRNA resulted in a significant reduction in LSCC cell growth (**Figure 1E**). Δp63 and c-Jun -critical factors in squamous cell identity and tumor maintenance, respectively- were also evaluated by IHC and exhibited the highest protein abundance in LSCC compared to LADC tumors (**Figure 1C, 1D**).

As c-Myc, c-Jun and Δp63 protein levels are controlled by the deubiquitinase Usp28 (Popov et al., 2007; Prieto-Garcia et al., 2020), we analysed its expression in publicly available datasets (The Cancer Genome Atlas). We observed that 25% of human LSCC cases show gain-of-function alterations in *USP28* (**Figure 1F**). qPCR analysis on human lung biopsy samples confirmed that *USP28* is highly expressed in LSCC tumors compared to healthy lung tissue (**Figure 1G**). Since Usp28 is involved in Δp63, c-Jun and c-Myc stabilization and higher expression of USP28 is associated with a significantly shorter survival time (Prieto-Garcia et al., 2020), we targeted its expression. Usp28 downregulation by shRNA resulted in a significant reduction in c-Myc, c-Jun and Δp63 protein levels in LSCC primary tumor cells and reduced LSCC

cell growth (**Figure 1H, 1I**). Thus, targeting Usp28 in order to destabilize its substrates represents a rational strategy to target tumor cells that rely on oncogenic transcription factors that are currently not druggable by small molecules.

Generation of a pre-clinical dual recombinase lung cancer mouse model

Recently, Usp28 was shown to be required for the initiation of lung tumors in the Rosa26-Cas9 sgRNA $Kras^{G12D}$; Tp53; Lkb1 model (Prieto-Garcia et al., 2020). However, a meaningful pre-clinical model requires targeting the therapeutic candidate gene in existing growing lung tumors. Thus, to assess the function of *Usp28* in established tumors, we developed a new genetically engineered mouse (GEM) model to temporally and spatially separate tumor development from target deletion by using two independent recombinases: Flp and Cre^{ERT}. In this model, LSCC and LADC formation is initiated by $KRas^{G12D}$ activation and *Fbxw7* deletion using Flp recombinase, and the Cre/loxP system can then be used for inactivation of $Usp28^{flox/flox}$ in established tumors. To allow conditional FRT/Flp-mediated inactivation of Fbxw7 function, we inserted two FRT sites flanking exon 5 of the endogenous Fbxw7 gene in mice to generate a $Fbxw7^{FRT/FRT}$ allele that can be deleted by Flp recombinase (**Figure S1A, S1B**). Expression of Flp recombinase resulted in the deletion of *Fbxw7* exon 5, which could be detected by PCR (**Figure S1B**). The resulting strain, $Fbxw7^{FRT/FRT}$, was crossed to FRT-STOP-FRT (FSF)-$KRas^{G12D}$ mice to generate FSF-$KRas^{G12D}$; $Fbxw7^{FRT/FRT}$ (KF-Flp model).

Usp28 is an effective therapeutic target for LSCC, but not $KRas^{G12D}$; Trp53 mutant LADC tumors

The KF-Flp strain described above was crossed with ROSA26-FSF-Cre^{ERT}; Usp28$^{flox/flox}$ mice to generate the KFCU model (**Figure 2A**). KFCU tumor development was monitored by CT scans. At ten-to-eleven weeks post-infection with Flp recombinase-expressing recombinant adenoviruses, animals displayed lesions in their lungs. At this time point, we confirmed by histology that KFCU mice develop both LADC and LSCC tumors (**Figure S1C**). As expected (Ruiz et al., 2019), KFCU LADC lesions occurred in alveolar tissue and were positive for Sftpc and TTF1. KFCU LSCC tumors occurred mainly in bronchi (rarely manifesting in the alveolar compartment) and expressed CK5 and ΔNp63. Next, animals displaying lung tumors were exposed to tamoxifen to activate the Cre^{ERT} protein and delete the conditional *Usp28* floxed alleles (**Figure 2A**). Loss of Usp28 expression, which was confirmed by BaseScope assays, did not reduce the number of LADC tumors (**Figure 2B, 2C, 2G**). In contrast, histological examination of KFCU mice revealed a clear reduction in the numbers of LSCC lesions in *Usp28*-deleted lungs (**Figure 2B, 2E, 2G**). As well as a significant reduction in tumor number, the few CK5-positive LSCC lesions that remained were substantially smaller than control tumors (**Figure 2F**). Measurement of 195 individual KFCU LSCC tumors (141 vehicle-treated and 54 tamoxifen-treated) showed an average of $10.7x10^4$ μm^2 in the vehicle arm versus $4.9x10^4$ μm^2 in the tamoxifen arm (**Figure 2F).** To get insights into LSCC tumor regression, we focused on Usp28 substrates. Immunoblotting and IHC analysis revealed that Usp28 deletion resulted in apoptotic cell death concomitant with reduced ΔNp63 protein levels and c-Jun and c-Myc protein became undetectable (**Figure 2H, 2I**). Thus, USP28 and its substrates are required for the maintenance of LSCC tumors.

To confirm the absence of therapeutic benefit of *Usp28* inactivation in LADC in a second genetic model, we used Flp-inducible oncogenic K-Ras activation combined

with p53 deletion (FSF-KRas^{G12D} and Trp53$^{FRT/FRT}$ or KP-Flp model) (Schonhuber et al., 2014). The KP-Flp mice were crossed to a conditional Usp28$^{flox/flox}$ strain together with an inducible Cre^{ERT} recombinase knocked in at the ROSA26 locus and an mT/mG reporter allele (KPCU mice; **Figure 3A**). After intratracheal adeno-CMV-Flp virus instillation, *Usp28* was inactivated in KPCU animals displaying lung tumors by CT (**Figure 3B**). Loss of Usp28 expression in this second LADC model also did not result in a reduction of LADC tumor number (**Figure 3C, 3D**). Successful Cre^{ERT} recombination was verified using lineage tracing (GFP staining) and deletion of Usp28$^{flox/flox}$ alleles was further confirmed by BaseScope assays (**Figure 3C, 3E**). Therefore, these data suggest an important role for Usp28 in advanced LSCC, but not LADC, tumors.

Generation of a new Usp28 inhibitor: selectivity and cellular target engagement

The finding that Usp28 plays a key role in LSCC tumor maintenance prompted us to identify small molecule inhibitors against this deubiquitinase. A small molecule discovery campaign based on the ubiquitin-rhodamine cleavable assay (Turnbull et al., 2017) yielded a panel of compounds sharing a thienopyridine carboxamide chemical scaffold with inhibitory selectivity for USP28 and USP25 (Guerin, 2017). The compound FT206 represents a different chemical class from the benzylic amino ethanol-based inhibitors described previously (Wrigley et al., 2017). Its functional groups optimise its pharmacodynamics properties with EC50 values below 1μM based on activity-based probe assays. FT206 targets endogenous USP28 and USP25 at a cellular level as measured in an activity-based probe profiling (ABPP) assay (**Figure 4A, 4B**). Furthermore, using an ABPP assay combined with quantitative mass spectrometry profiling 28 DUBs revealed remarkable USP28/25 selectivity for FT206

(**Figure 4C**). Finally, treatment of primary LSCC tumor cells with FT206 resulted in reduced c-Myc, c-Jun and ΔNp63 protein levels and impaired cell growth (**Figure 4D, 4E**).

Pharmacological inhibition of Usp28 is well tolerated in mice and induced LSCC tumor regression

We next evaluated the therapeutic potential of the USP28 inhibitor FT206 using the LSL-KRas^{G12D}; Fbxw7$^{flox/flox}$ model (KF mice), which develop both LADC and LSCC tumor types (Ruiz et al., 2019). Nine weeks after adeno-CMV-Cre virus infection, when mice had developed lung tumors, we started treatment with USP28 inhibitor at 75 mg/kg, 3 times a week for 5 weeks (**Figure 5A**). FT206 administration had no noticeable adverse effects and treated mice maintained normal body weight (**Figure S2A, S2B**). Consistent with the effects observed by genetic Usp28 inactivation (**Figure 2C**), the number of KF LADC lesions was not affected by Usp28 inhibition via FT206 treatment (**Figure 5B, 5C, 5D**). By contrast, we found that FT206 effectively reduced LSCC tumor number by 68% (31 to 10 LSCC tumors, **Figure 5B, 5E**). Moreover, measurement of 252 individual KF LSCC mutant tumors (156 vehicle-treated and 96 FT206-treated lesions) showed a significant reduction of over 45% in tumor size upon FT206 treatment: an average of 8.5x10^4 μm^2 in the vehicle arm versus 4.5x10^4 μm^2 in the FT206 cohort (**Figure 5F**). Thus, Usp28 inhibition by FT206 leads to a dramatic reduction in the numbers of advanced LSCC tumors, and the small number of remaining LSCC lesions are significantly reduced in size, resulting in a reduction of total LSCC burden of over 85% by single agent treatment.

In line with the effects found by genetic Usp28 deletion, treatment of KF mice with FT206 also resulted in reduced ΔNp63, c-Jun and c-Myc protein levels (**Figure 5G**).

Consequently, FT206 treatment led to a substantial increase in the number of active caspase-3-positive cells in LSCC while LADC cells were not significantly affected, indicating that USP28 inhibition causes apoptotic cell death of LSCC tumor cells (**Figure 5H, 5I**).

Finally, to further confirm the specificity of FT206, KFCU mice pre-exposed to tamoxifen to delete the conditional *Usp28* floxed alleles were further treated with the USP28 inhibitor FT206. In this setting, Usp28 inhibition did not result in a further reduction of LADC and LSCC lesions (**Figure S3A-D**), suggesting that FT206 targets specifically Usp28.

USP28 inhibition causes dramatic regression of human LSCC xenograft tumors

To determine whether the promise of Usp28 as a target in mouse lung cancer models can be translated to a human scenario, we established human xenograft tumor models. siRNA-mediated USP28 depletion, and USP28 inhibitor treatment, considerably reduced protein levels of ΔNp63, c-Jun and c-Myc and impaired growth in human LSCC tumor cells (**Figure 6A-C, S2C**). Crucially, FT206 led to a remarkable growth impairment of xenografts derived from three independent human LSCC cell lines (**Figure 6D-I**), which was accompanied with a strong reduction of c-Myc protein levels (**Figure 6J-L**). In summary, these data suggest that USP28 pharmacological intervention is a promising therapeutic option for human LSCC patients.

Discussion

Unlike for LADC, there are few approved targeted therapies against LSCC. Consequently, despite its limited effectiveness on disease progression and prognosis, patients with LSCC receive the same conventional platinum-based chemotherapy today as they would have received two decades ago (Fennell et al., 2016; Gandara et al., 2015; Isaka et al., 2017; Liao et al., 2012; Scagliotti et al., 2008).

c-MYC is a transcription factor that orchestrates a potent pro-cancer programme across multiple cellular pathways. As c-MYC is often overexpressed in late-stage cancer, targeting it for degradation is an attractive strategy in many settings. The term 'undruggable' was coined to describe proteins that could not be targeted pharmacologically. Many desirable targets in cancer fall into this category, including the c-MYC oncoprotein, and pharmacologically targeting these intractable proteins is a key challenge in cancer research.

The deubiquitylase family of enzymes have emerged as attractive drug targets, that can offer a means to destabilize client proteins that might otherwise be undruggable (Schauer et al., 2019). The deubiquitinase Usp28 was known to remove Fbw7-mediated ubiquitination of, and thereby stabilise, the oncoprotein c-MYC (Popov et al., 2007). Importantly, mice lacking USP28 are healthy (Knobel et al., 2014), suggesting that Usp28 is dispensable for normal physiology and homeostasis.

In the current study we identified a requirement for USP28 for the maintenance of murine and human LSCC tumors. In agreement with the absence of major phenotypes in the *Usp28* knock out mice, USP28 inhibitor treatment was well tolerated by the experimental animals, while having a dramatic effect on LSCC regression. USP28 small molecule inhibition phenocopies the effects of USP28 deletion in LSCC regression, strongly suggesting on-target activity. However, we cannot exclude that

the inhibition of USP25 and possibly additional off-targets effects may contribute to the observed phenotype.

While USP28 inhibition resulted in profoundly reduced LSCC growth, the effect on LADC was modest. TP63, c-Jun and c-Myc protein levels are increased in LSCC compared to LADC (**Figure 1C, 1D**). This could indicate a greater dependence of LSCC on these oncoproteins, which consequently may result in increased sensitivity to USP28 inhibition. We previously found that *usp28* deficiency corrected the accumulation of SCF(Fbw7) substrate proteins, including c-Jun and c-Myc, in *fbw7*-mutant cells (Diefenbacher et al., 2015). The frequent downregulation of *FBXW7* in human LSCC may underlie the increased accumulation of SCF(Fbw7) substrate proteins like c-Myc, c-Jun and p63 in LSCC, and thereby cause LSCC tumors to be increasingly dependent on USP28 function.

In summary, our studies demonstrate that USP28 is a key mediator of LSCC maintenance and progression and hence USP28 represents an exciting therapeutic target. Therefore, USP28 inhibition should be considered as a potential therapy for human lung squamous cell carcinoma.

Methods and Materials

Mice

The LSL-KRas^{G12D} (Jackson et al., 2001), Fbxw7$^{flox/flox}$ (Jandke et al., 2011), Usp28$^{flox/flox}$ (Diefenbacher et al., 2014), FSF-KRas^{G12D} (Schonhuber et al., 2014), Trp53$^{FRT/FRT}$ (Schonhuber et al., 2014), ROSA26-FSF-Cre^{ERT} (Schonhuber et al., 2014), ROSA26-LSL-mTmG (Muzumdar et al., 2007) strains have been previously described. Immunocompromised NSG mice were maintained in-house. All animal experiments were approved by the Francis Crick Institute Animal Ethics Committee and conformed to UK Home Office regulations under the Animals (Scientific Procedures) Act 1986 including Amendment Regulations 2012. All strains were genotyped by Transnetyx.

Generation of Fbxw7$^{FRT/FRT}$ Mice

To generate a conditional allele of Fbxw7, we employed the CRISPR-Cas9 approach to insert two FRT sites into the intron 4 and 5 of Fbxw7, respectively. Two guide RNAs targeting the integration sites (gRNA-Int5A: accgtcggcacactggtcca; gRNA-Int4A: cactcgtcactgacatcgat), two homology templates containing the FRT sequences (gRNA-Int5B: agcactgacgagtgaggcgg; gRNA-Int4B: tgcctagccttttacaagat) and the Cas9 protein were micro-injected into the fertilised mouse eggs. The offspring were screened by PCR and one line with proper integration of two FRT sites was identified.

Analysis of TCGA data

Data from TCGA Research Network (TCGA Lung Adenocarcinoma and Lung Squamous Cell Carcinoma sample sets), including mutations, putative copy-number alterations, and mRNA z-scores (RNA Seq V2 RSEM; threshold 2.0), were analyzed

using cBioportal software and visualized using the standard Oncoprint output (Cerami et al., 2012).

Human lung tumor analysis

Human biological samples were collected, stored, and managed by the Cordoba node belonging to the Biobank of the Andalusian Health Service (Servicio Andaluz de Salud-SAS) and approved by the Ethics and Clinical Research Committee of the University Hospital Reina Sofia. All subjects gave informed consent. Pathologists assessed all samples before use. mRNA extracted from the samples was analyzed by qPCR. Primers are listed in Table 1.

Tumor induction and tamoxifen treatment

Induction of NSCLC tumors was carried out in anesthetized (2-2.5% isoflurane) 8-to-12-week old mice by intratracheal instillation of a single dose of $2.5x10^7$ pfu of adenoviruses encoding either the Cre recombinase (adeno-CMV-Cre) or Flp recombinase (adeno-CMV-Flp). Activation of the inducible Cre^{ERT2} recombinase was carried out by intraperitoneal injection of tamoxifen (100 μg/kg body weight) dissolved in peanut oil for 10 days.

CT image acquisition and processing

The SkyScan-1176, a high-resolution low-dose X-ray scanner, was used for 3D computed tomography (CT). Mice were anesthetized with 2-2.5% isoflurane and CT images were acquired at a standard resolution (35 μm pixel size). The raw scan data was sorted using RespGate software, based on the position of the diaphragm, into

end expiration bins. 3D reconstruction was performed using NRecon software. 3D data sets were examined using Data Viewer software.

Mouse treatments with FT206

Nine-weeks upon Ad5-CMV-Cre infection, LSL-KRas^{G12D}; Fbxw7$^{flox/flox}$ mice were treated with FT206 (75 mg/kg) via oral gavage on day 1, 3, and 5 per week during 5 weeks. Body weights were register every week.

In vivo pharmacology with subcutaneous graft tumors

Human LSCC tumor cell lines (NCI-H520, CALU-1 and LUDLU-1) were resuspended as single-cell suspensions at 10^7 cells/ml in PBS:Matrigel. 100 μl (10^6 cells total) of this suspension was injected into the flanks of immunodeficient NSG mice. When tumors were palpable, treatment with FT206 (75 mg/kg) was initiated with the same schedule on day 1, 3, and 5 per week. Tumor grafts were measured with digital callipers, and tumor volumes were determined with the following formula: (length × width^2) × (π/6). Tumor volumes are plotted as means ± SD.

Histopathology, Immunohistochemistry and BaseScope analysis

For histological analysis, lungs were fixed overnight in 10% neutral buffered formalin. Fixed tissues were subsequently dehydrated and embedded in paraffin, and sections (4 μm) were prepared for H&E staining or IHC. Antibodies are given in Table 2. BaseScope was performed following the manufacturer's protocol. The *Usp28*-specific probe was custom-designed to target 436-482 of NM_175482.3; *Ppib* probe was used as a positive control (Bio-Techne Ltd).

Cell treatments

Mouse KF LSCC and human LUDLU-1 cells were treated with vehicle or FT206 at different concentrations for 48hr. Primary mouse KF LSCC cells were infected with inducible-shRNAs against the Usp28 gene and then expose to Doxycycline hyclate (1µg/ml) for 48h. Human LUDLU-1 cells were transfected with specific small interfering RNAs (siRNAs) against the USP28 gene, using Lipofectamine RNAiMAX and 25nM of each siRNA according to the manufacturer's instructions (Dharmacon).

Western Blot Analysis

Cells were lysed in ice-cold lysis buffer (20 mM Tris HCl, pH 7.5, 5 mM $MgCl_2$, 50 mM NaF, 10 mM EDTA, 0.5 M NaCl, and 1% Triton X-100) that was completed with protease, phosphatase, and kinase inhibitors. Protein extracts were separated on SDS/PAGE gel, transferred to a nitrocellulose membrane and blotted with antibodies are given in Table 2. Primary antibodies were detected against mouse or rabbit IgGs and visualized with ECL Western blot detection solution (GE Healthcare) or Odyssey infrared imaging system (LI-COR, Biosciences).

USP28 inhibitor synthesis

Synthesis and characterization of the USP28/25 small molecule inhibitor FT206, a thienopyridine carboxamide derivative, has been described previously (Guerin, 2017).

Cellular DUB profiling using Ub-based active site directed probes

Molecular probes based on the ubiquitin scaffold were generated and used essentially as described (Pinto-Fernandez et al., 2019; Turnbull et al., 2017). In brief, HA-tagged Ub bromoethyl (HA-UbC2Br) and HA-tagged Ub propargyl probes were synthesised

by expressing the fusion protein HA-Ub75-Intein-Chitin binding domain in E.Coli BL21 strains. Bacterial lysates were prepared and the fusion protein purified over a chitin binding column (NEB labs, UK). HA-Ub75-thioester was obtained by incubating the column material with mercaptosulfonate sodium salt (MESNa) overnight at 37°C. HA-Ub75-thioester was concentrated to a concentration of ~1mg/ml using 3,000 MW filters (Sartorius) and then desalted against PBS using a PD10 column (GE Healthcare). 500 µL of 1-2mg/mL of HA-Ub75- thioester was incubated with 0.2mmol of bromo-ethylamine at pH 8-9 for 20 minutes at ambient temperature, followed by a desalting step against phosphate buffer pH 8 as described above. Ub probe material was concentrated to ~1mg/ml, using 3,000 MW filters (Sartorius), and kept as aliquots at -80°C until use.

DUB profiling competition assays with cell extracts and with cells

Crude MCF7 cell extracts were prepared as described previously using glass-bead lysis in 50mM Tris pH 7.4, 5mM $MgCl_2$, 0.5mM EDTA, 250mM sucrose, 1mM DTT. For experiments with crude cell extracts, 50 µg of MCF7 cell lysate was incubated with different concentrations of USP28 inhibitor compounds (FT206) for one hour at 37°C, followed by addition of ~1µg HA-UbC2Br or ~1µg HA-UbPA and incubation for 5 minutes at 37°C. Incubation with Ub-probe was optimised to minimise replacement of non-covalent inhibitor FT206 by the covalent probe. Samples were then subsequently boiled in reducing SDS-sample buffer, separated by SDS-PAGE and analysed by Western Blotting using anti-HA (Roche, 1:2000), anti-USP28 (Abcam, 1:1000), anti-USP25 (Abcam, 1:1000), anti-USP36 (Abcam, 1:1000), anti-USP7 (Enzo, 1:1000), anti-USP11 (Abcam, 1:1000), anti-GAPDH (Invitrogen, 1:1000) or beta Actin (Abcam, 1:2000) antibodies. For cell-based DUB profiling, $5x10^6$ intact MCF7 cells were

incubated with different concentrations of inhibitors in cultured medium for 4 hours at 37°C, followed by glass-bead lysis, labelling with HAUbC2PA probe, separation by SDS-PAGE and Western blotting as described above.

DUB inhibitor profiling by quantitative mass spectrometry

Ub-probe pulldown experiments in presence of different concentrations of the inhibitor FT206 were performed essentially as described (Pinto-Fernandez et al., 2019; Turnbull et al., 2017) with some modifications. In brief, immune precipitated material from 500µg-1mg of MCF-7 cell crude extract was subjected to in-solution trypsin digestion and desalted using C18 SepPak cartridges (Waters) based on the manufacturer's instructions. Digested samples were analyzed by nano-UPLC-MS/MS using a Dionex Ultimate 3000 nano UPLC with EASY spray column (75µm x 500 mm, 2µm particle size, Thermo Scientific) with a 60 minute gradient of 0.1% formic acid in 5% DMSO to 0.1% formic acid to 35% acetonitrile in 5% DMSO at a flow rate of ~250nl/min (~600bar/40°C column temperature). MS data was acquired with an Orbitrap Q Exactive High Field (HF) instrument in which survey scans were acquired at a resolution of 60.000 @ 400m/z and the 20 most abundant precursors were selected for CID fragmentation. From raw MS files, peak list files were generated with MSConvert (Proteowizard V3.0.5211) using the 200 most abundant peaks/spectrum. The Mascot (V2.3, Matrix Science) search engine was used for protein identification at a false discovery rate of 1%, mass deviation of 10ppm for MS1 and 0.06 Da (Q Exactive HF) for MS2 spectra, cys carbamidylation as fixed modification, met oxidation and Gln deamidation as variable modification. Searches were performed against the UniProtKB human sequence data base (retrieved 15.10.2014). Label-free quantitation was performed using MaxQuant Software (version 1.5.3.8), and data further analysed

using GraphPad Prism software (v7) and Microsoft Excel. Statistical test-s ANOVA (multiple comparison; Original FRD method of Benjamini and Hochberg) was performed using GraphPad Prism software.

Statistical analysis

Data are represented as mean ± SD. Significance was calculated with the unpaired Student's t test, one-way or two-way ANOVA using GraphPad Prism software. A *P* value that was less than 0.05 was considered to be statistically significant for all data sets. Significant differences between experimental groups were: *p< 0.05, **p< 0.01 or *** p< 0.001.

Acknowledgements

Part of this work was funded by Forma Therapeutics. This work was also supported by the Francis Crick Institute which receives its core funding from Cancer Research UK (FC001039), the UK Medical Research Council (FC001039), and the Wellcome Trust (FC001039). We thank the Discovery Proteomics Facility (led by Dr Roman Fischer) at the Target Discovery Institute (Oxford) for expert help with the analysis by mass spectrometry. Work in the B.M.K. laboratory was supported by a John Fell Fund 133/075, the Wellcome Trust (097813/Z/11/Z) and the Engineering and Physical Sciences Research Council (EP/N034295/1).

Author Contributions

EJR, CJD, TRH, SK, DK, SU, MJC, BMK and AB designed the study. EJR, LL, EMR, CDC, IR, DS and EN performed mouse genetics and in vivo experiments. EJR, TMC, AD, GV, HCS and APF performed biochemical experiments. APT and WWK performed the structural analysis, which was amended by MG, BMK and DK. DG, JK, SI and KKB designed and characterised small molecule inhibitors. All authors commented on the manuscript. EJR, APF, APT, BMK and AB wrote the manuscript.

Declaration of Interests

The authors declare competing financial interests due to financial support for the project described in this manuscript by Forma Therapeutics, Watertown, MA, USA.

Figure legends

Figure 1. MYC, JUN and ΔNp63 are highly expressed in LSCC tumors

A) Expression of MYC in human lung adenocarcinoma (LADC, n = 483), lung squamous cell carcinoma (LSCC, n = 486), and normal non-transformed tissue (normal LSCC = 338, normal LADC = 347). In box plots, the centre line reflects the median. Data from TCGA and GTEx were analyzed using GEPIA software.

B) Relative mRNA expression of MYC in normal lung tissue (n = 5) and LSCC (n = 17) patient samples from the Cordoba Biobank measured by RT-PCR. The P value was calculated using the Student's two-tailed t test. Plots indicate mean.

C) Representative LADC and LSCC tumors stained with c-Myc, c-Jun and ΔNp63 antibodies. Bars, 30 μm.

D) Quantification of c-Myc$^+$ (LADC n = 33, LSCC n = 34), c-Jun$^+$ (LADC n = 33, LSCC n = 33) and ΔNp63$^+$ cells (LADC n = 41, LSCC n = 41) in LADC and LSCC tumors. Plots indicate mean. Student's two-tailed t test was used to calculate P values.

E) Graph showing the difference in cell proliferation between control and MYC-depleted KF LSCC cells

F) Genetic alterations in USP28 gene in human LSCC. Each column represents a tumor sample (n = 179). Data from TCGA were analyzed using cBioportal software.

G) Relative mRNA expression of USP28 in normal lung tissue (n = 5) and LSCC (n = 17) patient samples from the Cordoba Biobank measured by RT-PCR. The P value was calculated using the Student's two-tailed t test. Plots indicate mean.

H) shRNA-mediated knockdown of Usp28 decreases c-Myc, c-Jun and ΔNp63 protein levels in primary KF LSCC cells.

I) Graph showing the difference in cell proliferation between control and Usp28-depleted KF LSCC cells.

Figure 2. Usp28 is an effective therapeutic target for LSCC tumors

A) Schematic representation of the KFCU (FSF-KRas^{G12D}; Fbxw7$^{FRT/FRT}$; ROSA26-FSF-Cre^{ERT}; Usp28$^{flox/flox}$) model and experimental approach used to deplete conditional Usp28 alleles in established lung tumors.

B) Lung histology of animals treated as in A, showing both LSCC (CK5^{+}) and LADC (Sftpc^{+}) tumors in mice receiving vehicle but few LSCC lesions in mice receiving tamoxifen. Bars, 1000 μm.

C) Quantification of LADC tumors in vehicle- and tamoxifen-treated KFCU mice. Plots indicate mean. Student's two-tailed t test was used to calculate P values. (n = 5 vehicle, n = 4 tamoxifen)

D) Quantification of LADC tumor size in vehicle- and tamoxifen-treated KFCU mice. Plots indicate mean. Student's two-tailed t test was used to calculate P values (n = 181 vehicle, n = 196 tamoxifen).

E) Quantification of LSCC tumors in vehicle- and tamoxifen-treated KFCU mice. Plots indicate mean. Student's two-tailed t test was used to calculate P values (n = 5 vehicle, n = 4 tamoxifen).

F) Quantification of LSCC tumor size in vehicle- and tamoxifen-treated KFCU mice. Plots indicate mean. Student's two-tailed t test was used to calculate P values (n = 141 vehicle, n = 54 tamoxifen).

G) In situ hybridization of USP28 and PPIB mRNA expression in vehicle- and tamoxifen-treated KFCU mice. Scale bars, 50 μm

H) KFCU tumors stained with c-Myc, c-Jun and Δp63 antibodies. KFCU mice treated with vehicle (left panel) or tamoxifen (right panel). Inserts showing c-Myc^{+}, c-Jun^{+} and

$\Delta p63^{+}$ LSCC tumors in mice receiving vehicle but partial positive or negative LSCC lesions in mice receiving tamoxifen. Bars, 50 μm.

I) Usp28 deletion induces apoptotic cell death (caspase-3-active, C3A) and decreases c-Myc, c-Jun and $\Delta p63$ protein levels.

See also Supplementary Figure S2.

Figure 3. Usp28 is not a therapeutic target for advanced $KRas^{G12D}$; Trp53 mutant tumors

A) Schematic representation of the KPCU (FSF-$\underline{K}Ras^{G12D}$; $\underline{p}53^{FRT/FRT}$; ROSA26-FSF-$\underline{C}re^{ERT}$; $\underline{U}sp28^{flox/flox}$; ROSA26-LSL-mTmG) model.

B) Schematic illustration of the experimental approach used. At 10-weeks post-infection, KPCU mice were treated with vehicle or tamoxifen.

C) Representative images of H&E (left) and GFP (right) stains from mice of the indicated treatments. Scale bar, 1000 μm.

D) Quantification of mouse LADC tumors in the KPCU model. Plots indicate mean. Student's two-tailed t test was used to calculate P values (n = 10 vehicle, n = 10 tamoxifen).

E) Representative images illustrating histological analysis of lung lesions in KPCU mice, treated with vehicle or tamoxifen. H&E, Sftpc, TTF1, GFP immunohistochemistry staining and in situ hybridization of USP28 and PPIB mRNA expression. Scale bars, 50 μm.

Figure 4. USP28 inhibitor selectivity and cellular target engagement

A) Cellular DUB profiling in NCI-H520 LSCC cell extracts incubated with the indicated concentrations of FT206 prior to labelling with HA-UbPA, SDS-PAGE and analysis by Western blotting.

B) Cellular DUB profiling in NCI-H520 LSCC cells incubated with the indicated concentrations of FT206, lysed extracts labelled with HA-UbPA and analysed as in B.

C) Activity-based Probe Profiling (ABPP) demonstrating the cellular DUB selectivity profile of cpd FT206 by quantitative mass spectrometry analysis at different inhibitor concentrations.

D) Usp28 inhibition using FT206 (50nM and 100nM) reduces c-Myc, c-Jun and ΔNp63 protein levels in primary KF LSCC cells.

E) Usp28 inhibition using FT206 decreases cell proliferation in KF LSCC cells.

See also Supplementary Figure S3 and S4.

Figure 5. Pharmacologic USP28 inhibition reduces c-Myc, c-Jun and ΔNp63 protein levels in mouse LSCC tumors, and induces tumor cell death

A) Scheme depicting experimental design for in vivo test of FT206 (75mg/kg), 3 times a week for 5 weeks.

B) Lung histology of animals treated as in A, showing both LSCC ($CK5^+$) and LADC ($Sftpc^+$) tumors in LSL-$KRas^{G12D}$; $Fbxw7^{f/f}$ (KF) mice receiving vehicle but few LSCC lesions in mice receiving FT206. Bars, 1000 μm.

C) Quantification of LADC tumors per animal in vehicle- and FT206-treated KF mice. Plots indicate mean. P values calculated using Student's two-tailed t test (n = 7 vehicle, n = 10 FT206).

D) Quantification of LADC tumor size in vehicle- and FT206-treated KF mice. Plots indicate mean. Student's two-tailed t test was used to calculate P values (n = 304 vehicle, n = 481 FT206).

E) Quantification of LSCC tumors per animal in vehicle- and FT206-treated KF mice. Plots indicate mean. P values calculated using Student's two-tailed t test (n = 7 vehicle, n = 10 FT206).

F) Quantification of LSCC tumor size in vehicle- and FT206-treated KF mice. Plots indicate mean. Student's two-tailed t test was used to calculate P values (n = 156 vehicle, n = 96 FT206).

G) LSCC tumors stained with c-Myc, c-Jun and ΔNp63 antibodies. KF animals treated with vehicle (left panel) or FT206 (right panel). Inserts showing c-Myc$^+$, c-Jun$^+$, ΔNp63$^+$ LSCC tumors in mice receiving vehicle (left panel) but partial positive or negative LSCC lesions in mice receiving FT206 (right panel). Bars, 50 μm.

H) Scheme depicting experimental design for in vivo test of FT206 (75 mg/kg) for 4 days consecutively (upper panel). Active caspase-3 (C3A) stain shows apoptotic cells (bottom panel). Bars, 50 μm.

I) Quantification of active caspase-3 (C3A) in LADC and LSCC tumors from KF mice treated as in H. Plots indicate mean. Student's two-tailed t test was used to calculate P values.

Figure 6. Pharmacological inhibition of USP28 prevents human LSCC tumor progression and reduces c-Myc protein levels in xenograft models

A) siRNA-mediated knockdown of USP28 decreases c-Myc, c-Jun and ΔNp63 protein levels in human LUDLU-1 LSCC cells.

B) Usp28 inhibition using FT206 (0.4 and 0.8 μM) reduces c-Myc, c-Jun and Δp63 protein levels in human LUDLU-1 LSCC cells.

C) Usp28 inhibition using FT206 decreases cell proliferation in human LSCC (NCI-H520, CALU-1 and LUDLU-1) cell lines.

D, E, F) In vivo tumor graft growth curves of human LSCC (NCI-H520, CALU-1 and LUDLU-1) cell lines subcutaneously injected in flanks of immunocompromised mice. Animals with palpable tumors were treated with vehicle or FT206 (75mg/kg) via oral gavage. Plots indicate mean ± SD of the tumor volumes. P values calculated from two-way ANOVA (NCI-H520 n = 4 vehicle and 4 FT206; CALU-1 n = 3 vehicle and 3 FT206; LUDLU-1 n = 3 vehicle and 3 FT206).

G, H, I) Mice treated as in D, E and F, respectively. Plots showing the weight of xenograft tumors at the end point. Student's two-tailed t test was used to calculate P values (NCI-H520 n = 4 vehicle and 4 FT206; CALU-1 n = 3 vehicle and 3 FT206; LUDLU-1 n = 3 vehicle and 3 FT206).

J, K, L) c-Myc immunohistochemistry stainings of NCI-H520, CALU-1 and LUDLU-1 xenografts in mice treated as in D, E and F, respectively. Bars, 50 μm.

Supplementary figure legends

Supplementary Figure S1, related to Figure 2. Gene targeting strategy to generate a Fbxw7 FRT/FRT allele that can be deleted by Flp recombinase.

A) Gene targeting strategy to generate conditional Fbxw7$^{FRT/FRT}$ animals. Two FRT sites were inserted into the intron 4 and 5 of Fbxw7 through the CRISPR-Cas9 technology.

B) Schematic representation of the conditional allele (left panel). In vitro recombination assay demonstrated efficient ablation of the exon 5 upon Flp recombinase adenovirus infection (right panel).

D) KFCU (FSF-KRas^{G12D}; Fbxw7$^{FRT/FRT}$; ROSA26-FSF-Cre^{ERT}; Usp28$^{flox/flox}$) mice infected with adeno-CMV-Flp virus develop LADC (Sftpc^{+} and TTF1^{+}) and LSCC (CK5^{+} and Δp63^{+}) tumors.

Supplementary Figure S2, related to Figure 5.

A) Monitoring tolerability in mice treated with FT206 (75mg/kg), 3 times a week for 5 weeks. Body weights of animals during the course of treatment. (n = 3 vehicle, n = 3 FT206).

B) Kidney, liver and spleen sections stained with H&E. Mice treated as in A. Bars, 100 µm.

C) Usp28 inhibition using FT206 decreases cell proliferation in human LSCC (NCI-H226 and SKMES-1) cell lines.

Supplementary Figure S3, related to Figure 2 and 5.

A) Quantification of LADC tumors in vehicle-, tamoxifen- and tamoxifen+FT206 treated KFCU mice. Plots indicate mean. One-way ANOVA was used to calculate P values (n = 5 vehicle, n = 4 tamoxifen, n= 3 tamoxifen + FT206).

B) Quantification of LADC tumor size in vehicle-, tamoxifen- and tamoxifen+FT206 treated KFCU mice. Plots indicate mean. One-way ANOVA was used to calculate P values (n = 181 vehicle, n = 196 tamoxifen, n = 157 tamoxifen + FT206).

C) Quantification of LSCC tumors in vehicle-, tamoxifen- and tamoxifen+FT206 treated KFCU mice. Plots indicate mean. One-way ANOVA was used to calculate P values (n = 5 vehicle, n = 4 tamoxifen, n= 3 tamoxifen + FT206).

D) Quantification of LSCC tumor size in vehicle-, tamoxifen- and tamoxifen+FT206 treated KFCU mice. Plots indicate mean. One-way ANOVA was used to calculate P values (n = 141 vehicle, n = 54 tamoxifen, n = 29 tamoxifen + FT206).

References

Cancer Genome Atlas Research, N. (2012). Comprehensive genomic characterization of squamous cell lung cancers. Nature *489*, 519-525.

Cardarella, S., and Johnson, B. E. (2013). The impact of genomic changes on treatment of lung cancer. Am J Respir Crit Care Med *188*, 770-775.

Cerami, E., Gao, J., Dogrusoz, U., Gross, B. E., Sumer, S. O., Aksoy, B. A., Jacobsen, A., Byrne, C. J., Heuer, M. L., Larsson, E.*, et al.* (2012). The cBio cancer genomics portal: an open platform for exploring multidimensional cancer genomics data. Cancer Discov *2*, 401-404.

Davis, R. J., Welcker, M., and Clurman, B. E. (2014). Tumor suppression by the Fbw7 ubiquitin ligase: mechanisms and opportunities. Cancer Cell *26*, 455-464.

Diefenbacher, M. E., Chakraborty, A., Blake, S. M., Mitter, R., Popov, N., Eilers, M., and Behrens, A. (2015). Usp28 counteracts Fbw7 in intestinal homeostasis and cancer. Cancer Res *75*, 1181-1186.

Diefenbacher, M. E., Popov, N., Blake, S. M., Schulein-Volk, C., Nye, E., Spencer-Dene, B., Jaenicke, L. A., Eilers, M., and Behrens, A. (2014). The deubiquitinase USP28 controls intestinal homeostasis and promotes colorectal cancer. The Journal of clinical investigation *124*, 3407-3418.

Fennell, D. A., Summers, Y., Cadranel, J., Benepal, T., Christoph, D. C., Lal, R., Das, M., Maxwell, F., Visseren-Grul, C., and Ferry, D. (2016). Cisplatin in the modern era: The backbone of first-line chemotherapy for non-small cell lung cancer. Cancer Treat Rev *44*, 42-50.

Gandara, D. R., Hammerman, P. S., Sos, M. L., Lara, P. N., Jr., and Hirsch, F. R. (2015). Squamous cell lung cancer: from tumor genomics to cancer therapeutics. Clin Cancer Res *21*, 2236-2243.

Guerin, D., Bair, K., Caravella, J.A., Ioannidis, S., Lancia, D.R., Li, H., Mischke, S., Ng, P.Y., Richard, D., Schiller, S., et al. (2017). THIENOPYRIDINE CARBOXAMIDES AS UBIQUITIN-SPECIFIC PROTEASE INHIBITORS In USA: World Intellectual Property Organization International Bureau, (USA).

Hirsch, F. R., Govindan, R., Zvirbule, Z., Braiteh, F., Rittmeyer, A., Belda-Iniesta, C., Isla, D., Cosgriff, T., Boyer, M., Ueda, M.*, et al.* (2017). Efficacy and Safety Results From a Phase II, Placebo-Controlled Study of Onartuzumab Plus First-Line Platinum-Doublet Chemotherapy for Advanced Squamous Cell Non-Small-Cell Lung Cancer. Clin Lung Cancer *18*, 43-49.

Isaka, T., Nakayama, H., Yokose, T., Ito, H., Katayama, K., Yamada, K., and Masuda, M. (2017). Platinum-Based Adjuvant Chemotherapy for Stage II and Stage III Squamous Cell Carcinoma of the Lung. Ann Thorac Cardiovasc Surg *23*, 19-25.

Jackson, E. L., Willis, N., Mercer, K., Bronson, R. T., Crowley, D., Montoya, R., Jacks, T., and Tuveson, D. A. (2001). Analysis of lung tumor initiation and progression using conditional expression of oncogenic K-ras. Genes & development *15*, 3243-3248.

Jandke, A., Da Costa, C., Sancho, R., Nye, E., Spencer-Dene, B., and Behrens, A. (2011). The F-box protein Fbw7 is required for cerebellar development. Dev Biol *358*, 201-212.

Kan, Z., Jaiswal, B. S., Stinson, J., Janakiraman, V., Bhatt, D., Stern, H. M., Yue, P., Haverty, P. M., Bourgon, R., Zheng, J.*, et al.* (2010). Diverse somatic mutation patterns and pathway alterations in human cancers. Nature *466*, 869-873.

Knobel, P. A., Belotserkovskaya, R., Galanty, Y., Schmidt, C. K., Jackson, S. P., and Stracker, T. H. (2014). USP28 Is Recruited to Sites of DNA Damage by the Tandem BRCT Domains of 53BP1 but Plays a Minor Role in Double-Strand Break Metabolism. Molecular and cellular biology *34*, 2062-2074.

Liao, R. G., Watanabe, H., Meyerson, M., and Hammerman, P. S. (2012). Targeted therapy for squamous cell lung cancer. Lung Cancer Manag *1*, 293-300.

Muzumdar, M. D., Tasic, B., Miyamichi, K., Li, L., and Luo, L. (2007). A global double-fluorescent Cre reporter mouse. Genesis *45*, 593-605.

Novello, S., Scagliotti, G. V., Sydorenko, O., Vynnychenko, I., Volovat, C., Schneider, C. P., Blackhall, F., McCoy, S., Hei, Y. J., and Spigel, D. R. (2014). Motesanib plus carboplatin/paclitaxel in patients with advanced squamous non-small-cell lung cancer: results from the randomized controlled MONET1 study. J Thorac Oncol *9*, 1154-1161.

Pinto-Fernandez, A., Davis, S., Schofield, A. B., Scott, H. C., Zhang, P., Salah, E., Mathea, S., Charles, P. D., Damianou, A., Bond, G.*, et al.* (2019). Comprehensive Landscape of Active Deubiquitinating Enzymes Profiled by Advanced Chemoproteomics. Front Chem *7*, 592.

Popov, N., Wanzel, M., Madiredjo, M., Zhang, D., Beijersbergen, R., Bernards, R., Moll, R., Elledge, S. J., and Eilers, M. (2007). The ubiquitin-specific protease USP28 is required for MYC stability. Nat Cell Biol *9*, 765-774.

Prieto-Garcia, C., Hartmann, O., Reissland, M., Braun, F., Fischer, T., Walz, S., Schulein-Volk, C., Eilers, U., Ade, C. P., Calzado, M. A.*, et al.* (2020). Maintaining protein stability of Np63 via USP28 is required by squamous cancer cells. EMBO Mol Med *12*, e11101.

Ruiz, E. J., Diefenbacher, M. E., Nelson, J. K., Sancho, R., Pucci, F., Chakraborty, A., Moreno, P., Annibaldi, A., Liccardi, G., Encheva, V.*, et al.* (2019). LUBAC determines chemotherapy resistance in squamous cell lung cancer. J Exp Med *216*, 450-465.

Scagliotti, G. V., Parikh, P., von Pawel, J., Biesma, B., Vansteenkiste, J., Manegold, C., Serwatowski, P., Gatzemeier, U., Digumarti, R., Zukin, M.*, et al.* (2008). Phase III study comparing cisplatin plus gemcitabine with cisplatin plus pemetrexed in chemotherapy-naive patients with advanced-stage non-small-cell lung cancer. J Clin Oncol *26*, 3543-3551.

Schauer, N. J., Magin, R. S., Liu, X., Doherty, L. M., and Buhrlage, S. J. (2019). Advances in Discovering Deubiquitinating Enzyme (DUB) Inhibitors. J Med Chem.

Schonhuber, N., Seidler, B., Schuck, K., Veltkamp, C., Schachtler, C., Zukowska, M., Eser, S., Feyerabend, T. B., Paul, M. C., Eser, P.*, et al.* (2014). A next-generation dual-recombinase system for time- and host-specific targeting of pancreatic cancer. Nature medicine *20*, 1340-1347.

Turnbull, A. P., Ioannidis, S., Krajewski, W. W., Pinto-Fernandez, A., Heride, C., Martin, A. C. L., Tonkin, L. M., Townsend, E. C., Buker, S. M., Lancia, D. R.*, et al.* (2017). Molecular basis of USP7 inhibition by selective small-molecule inhibitors. Nature *550*, 481-486.

Wrigley, J. D., Gavory, G., Simpson, I., Preston, M., Plant, H., Bradley, J., Goeppert, A. U., Rozycka, E., Davies, G., Walsh, J.*, et al.* (2017). Identification and Characterization of Dual Inhibitors of the USP25/28 Deubiquitinating Enzyme Subfamily. ACS Chem Biol *12*, 3113-3125.

Table 1: Primers for qPCR

Name	**Primer (5′–3′)**	
	Forwad	Reverse
ACTIN	GAAAATCTGGCACCACACCT	TAGCACAGCCTGGATAGCAA
USP28	ACTCAGACTATTGAACAGATGTACTGC	CTGCATGCAAGCGATAAGG

Table 2: List of Reagents

REAGENT	**SOURCE**	**IDENTIFIER**
Antibodies		
Rabbit anti-CK5	Abcam	ab52635
Rabbit anti-c-Myc	Abcam	ab32072
Goat anti-GFP	Abcam	ab6673
Rabbit anti-Ki67	Abcam	ab16667
Rabbit anti-TTF1	Abcam	ab76013
Rabbit anti-USP28	Abcam	ab126604
Rabbit anti-USP25	Abcam	ab187156
Rabbit anti-USP11	Abcam	ab109232
Rabbit anti-USP36	Abcam	ab102565
Rabbit anti-actin	Abcam	ab8227
Rabbit anti-USP28	Atlas	HPA006779
Rabbit anti-ΔNp63	Biolegend	619001
Mouse anti-c-Jun	BD Biosciences	610326
Rabbit anti-USP7	Enzo	BML-PW0540
Mouse anti-GAPDH	Invitrogen	MA5-15738
Rabbit anti-Sftpc	Millipore	ab3786
Rabbit anti-caspase 3 active	R&D Systems	AF835
Rat anti-HA	Roche	11666606001
Mouse anti-tubulin	Sigma	T5168
Virus Strains		
Adeno-CMV-Cre	UI viral vector core	VVC-U of Iowa-5-HT
Adeno-CMV-Flp	UI viral vector core	VVC-U of Iowa-530HT
Chemicals, Peptides, and Recombinant Proteins		
Doxycycline hyclate	Sigma	D9891
Tamoxifen	Sigma	T5648

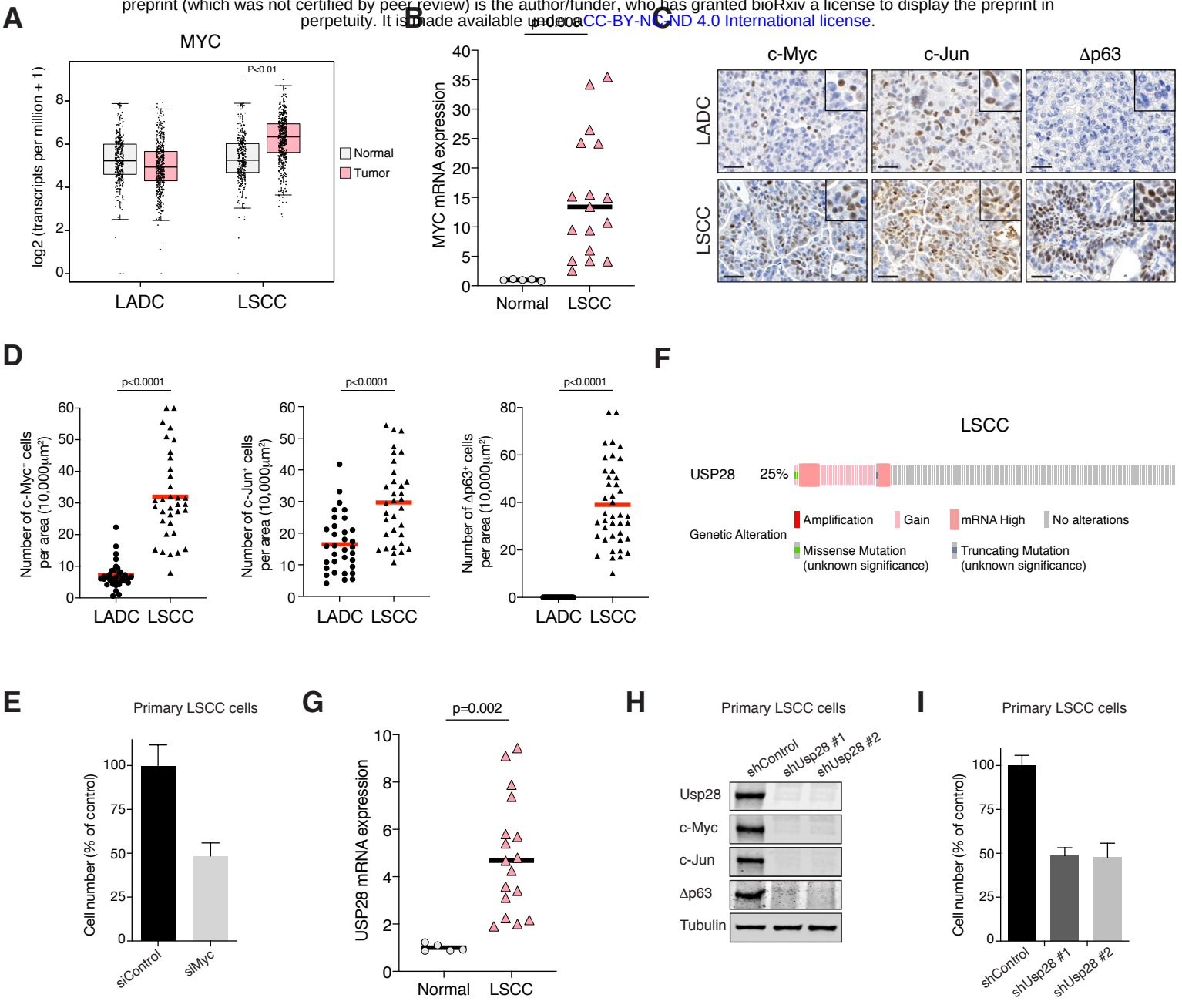

Figure 1

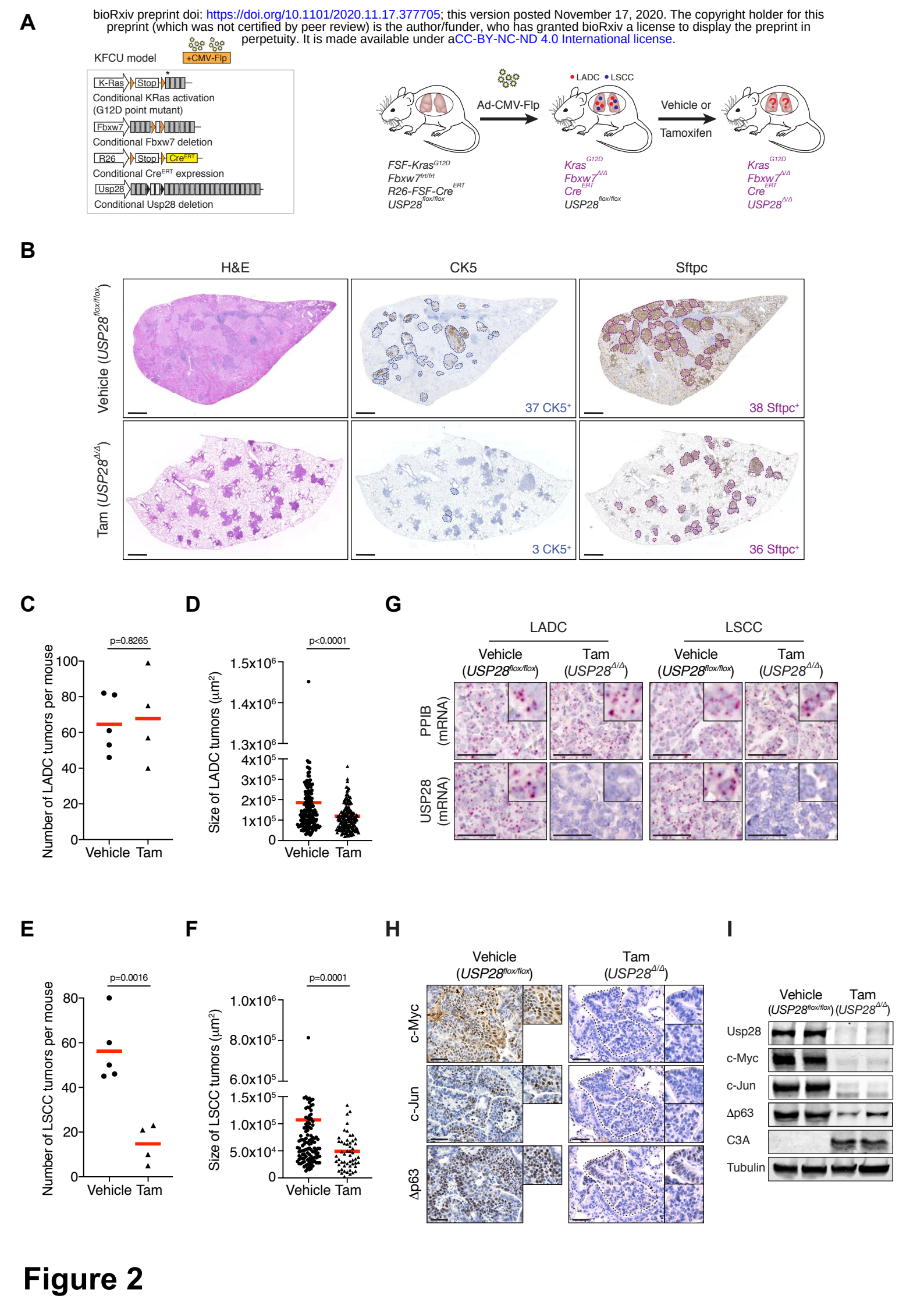

Figure 2

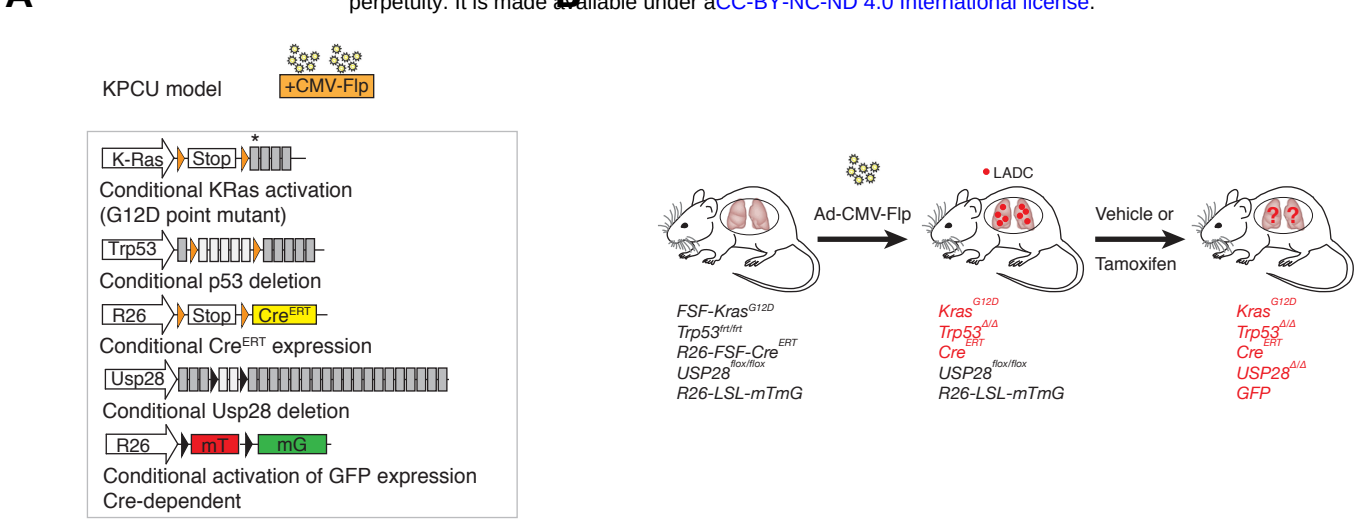

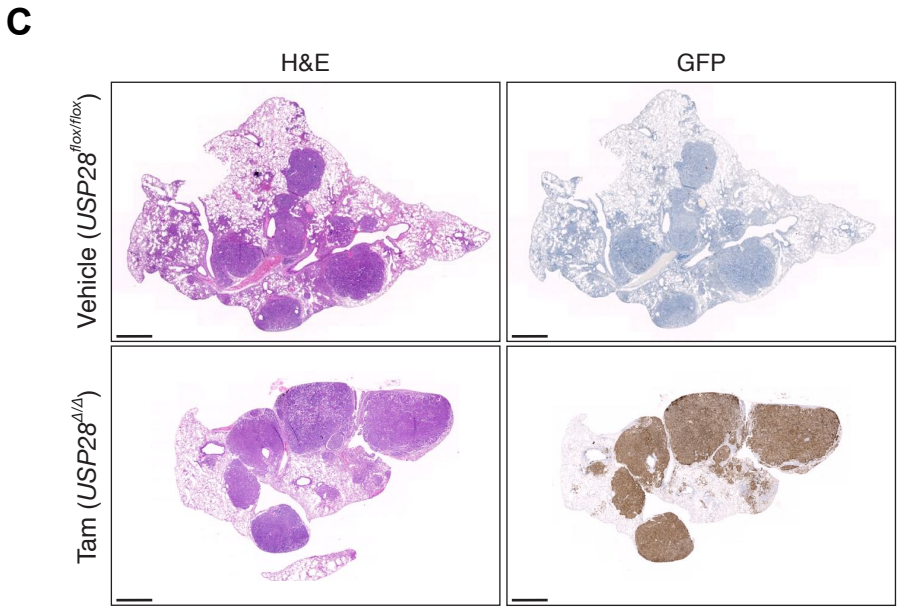

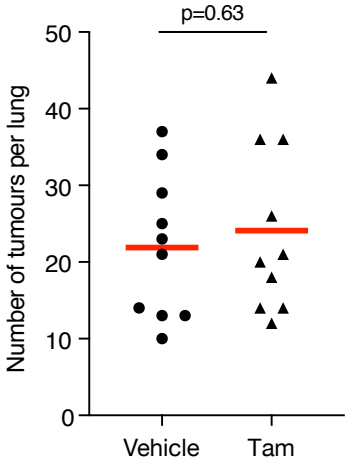

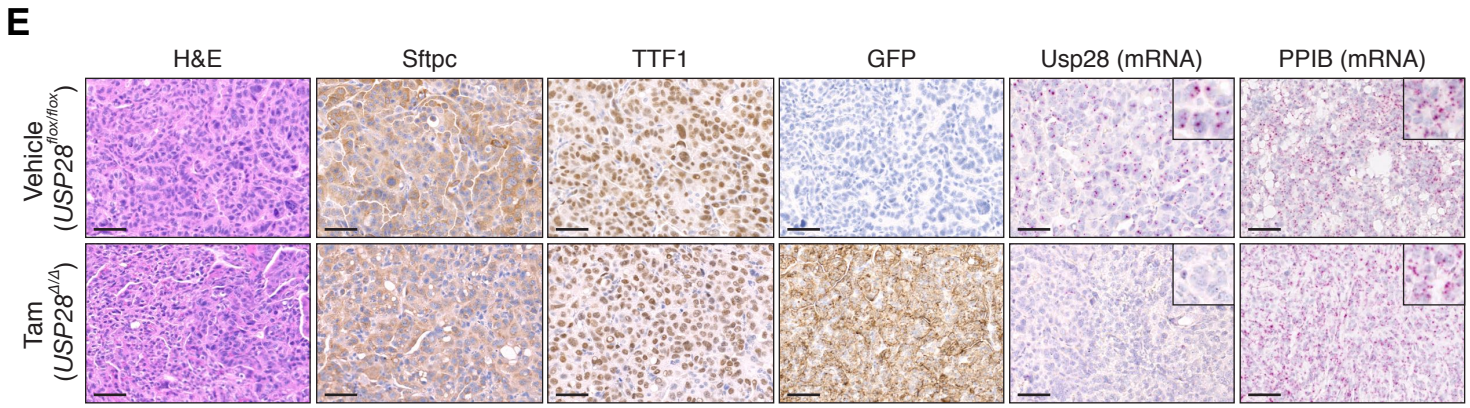

Figure 3

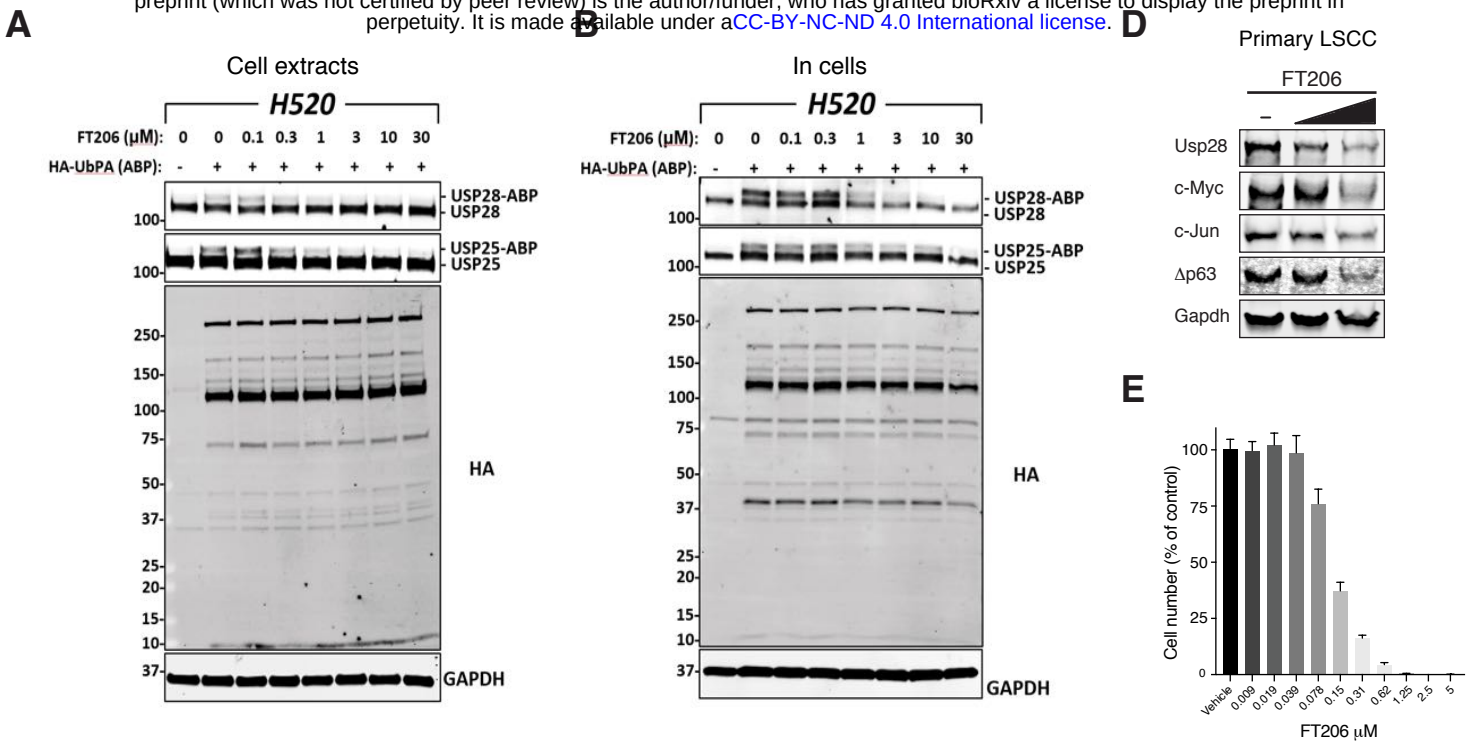

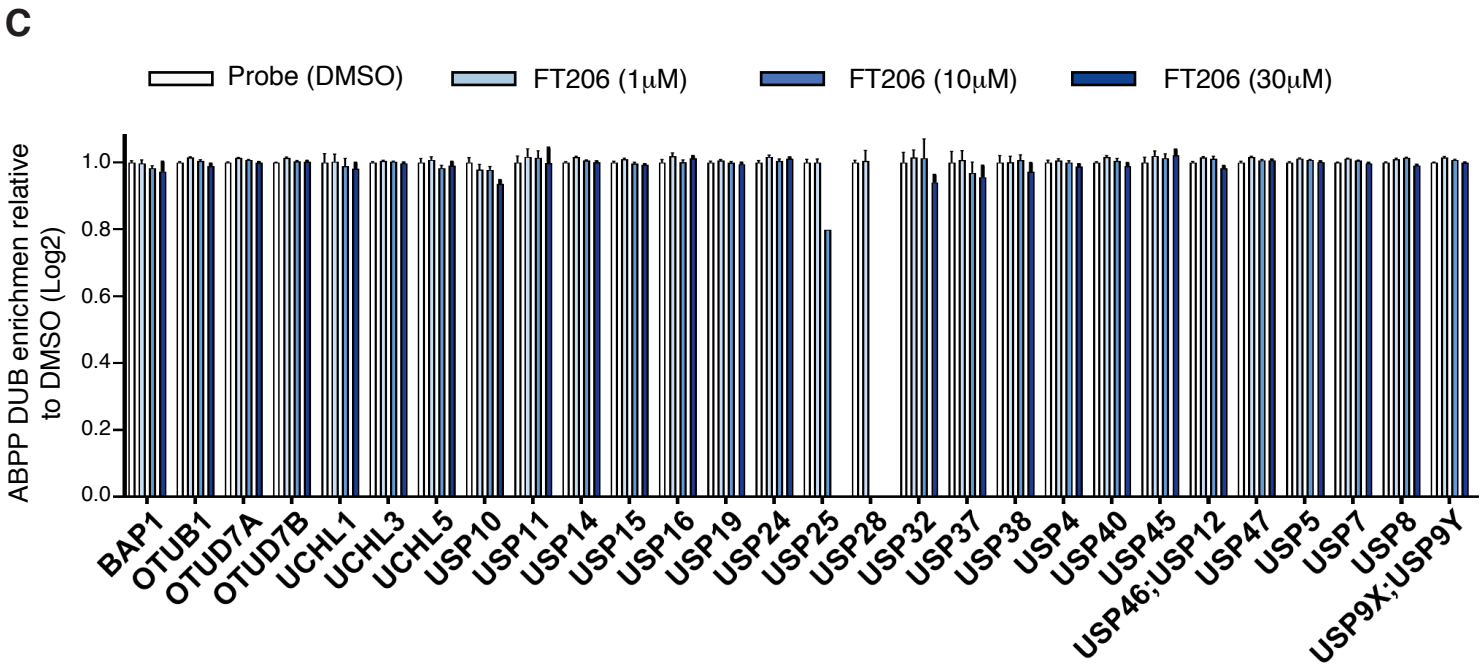

Figure 4

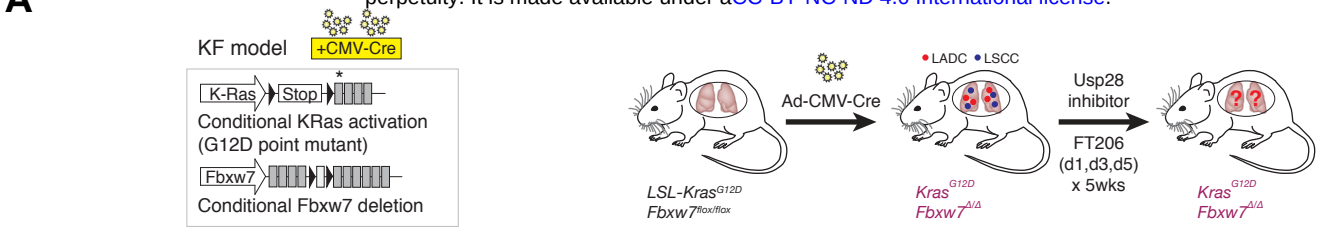

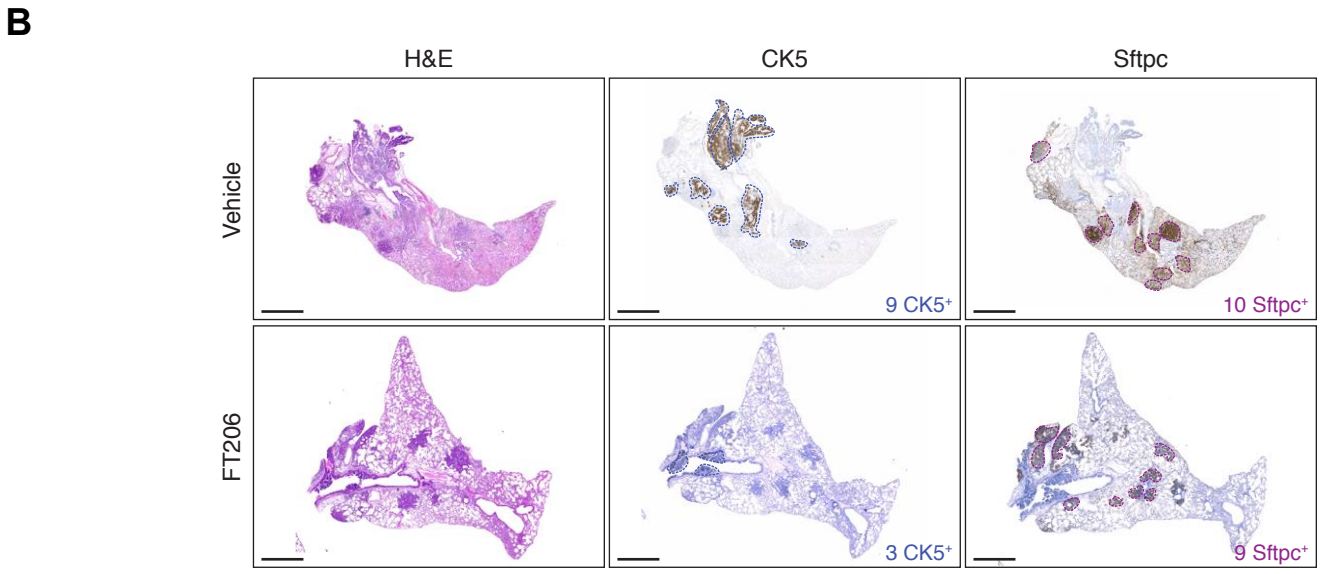

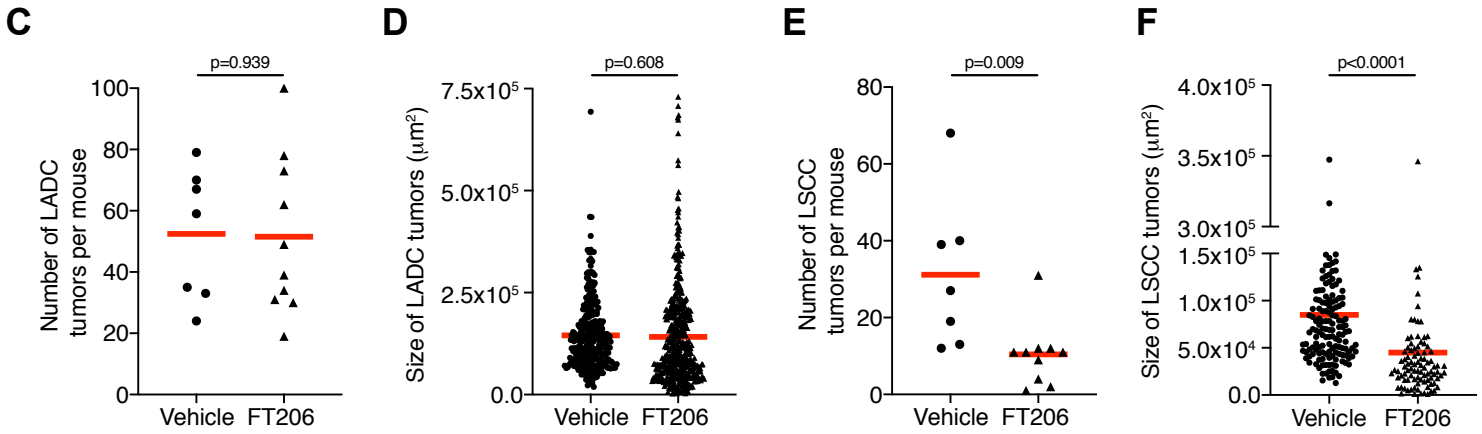

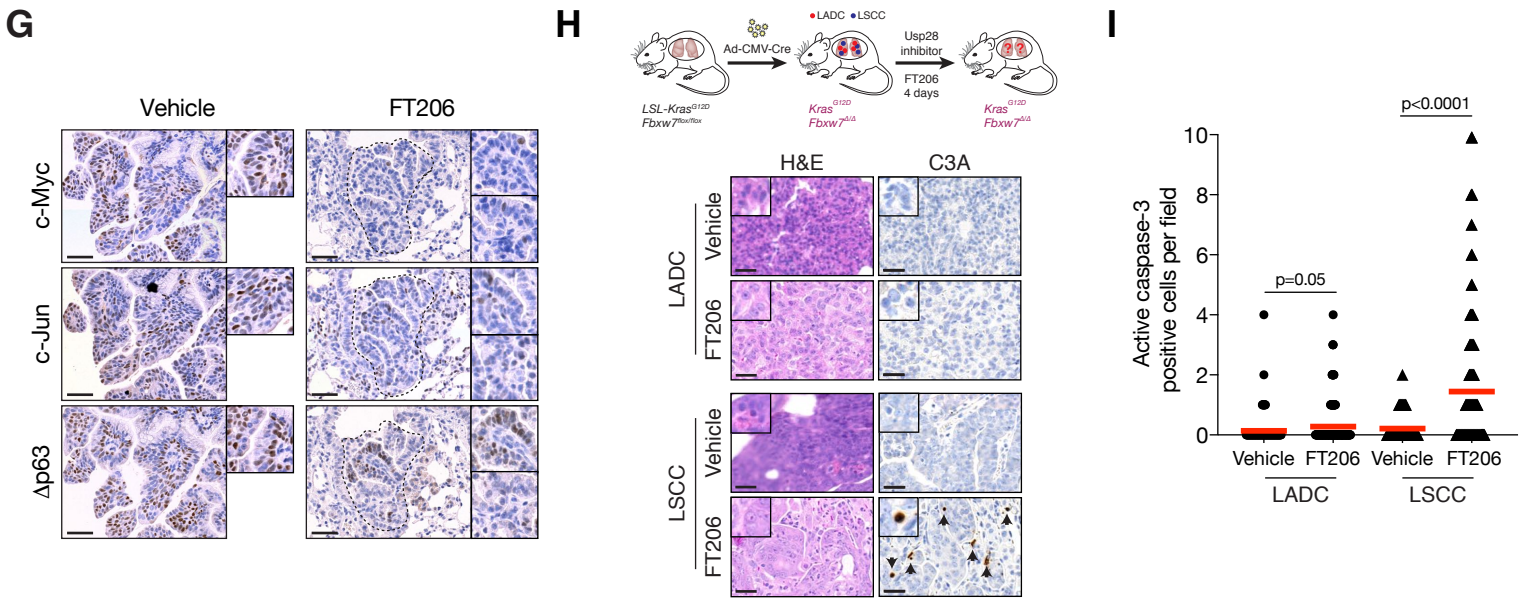

Figure 5

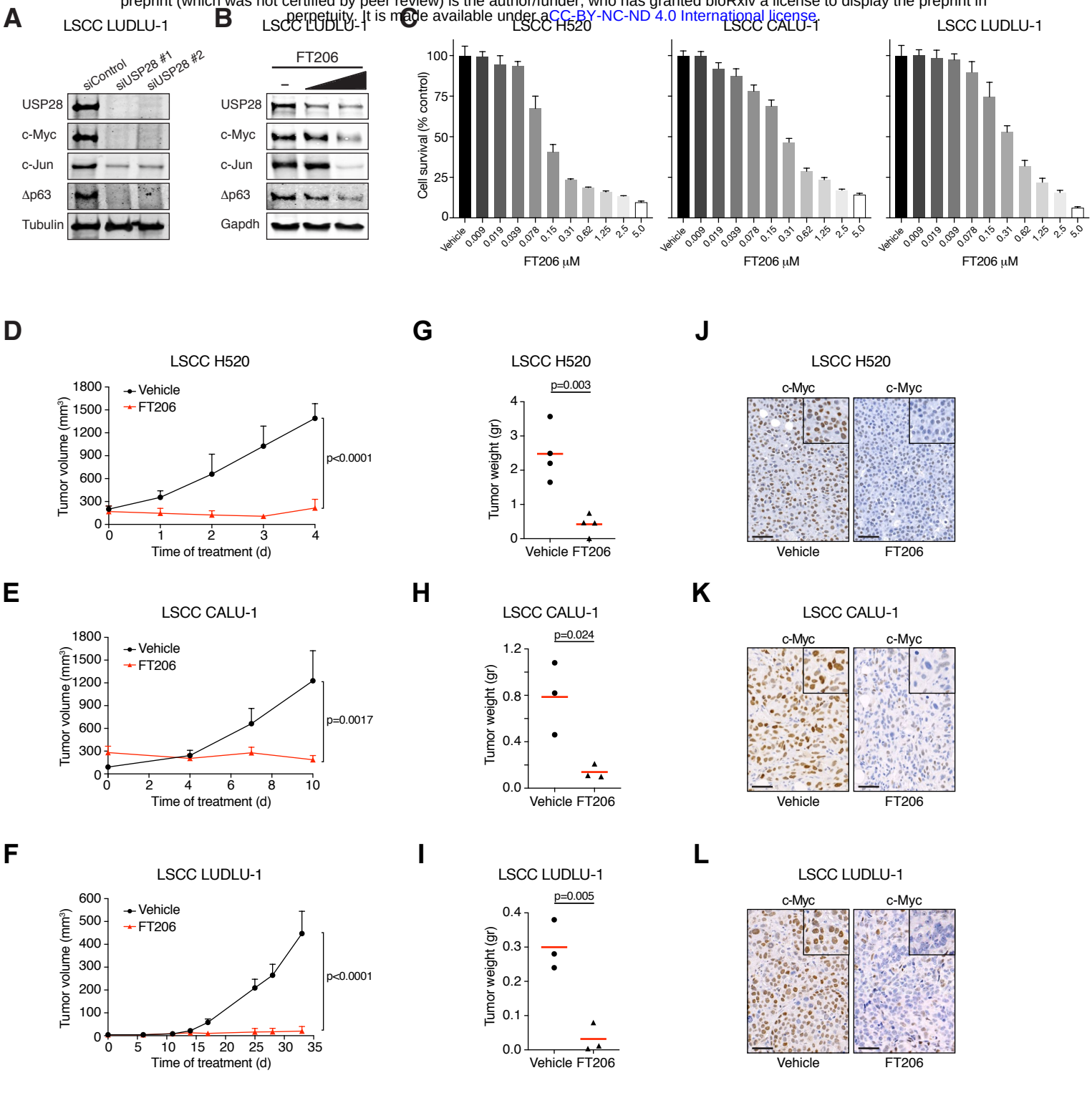

Figure 6

A

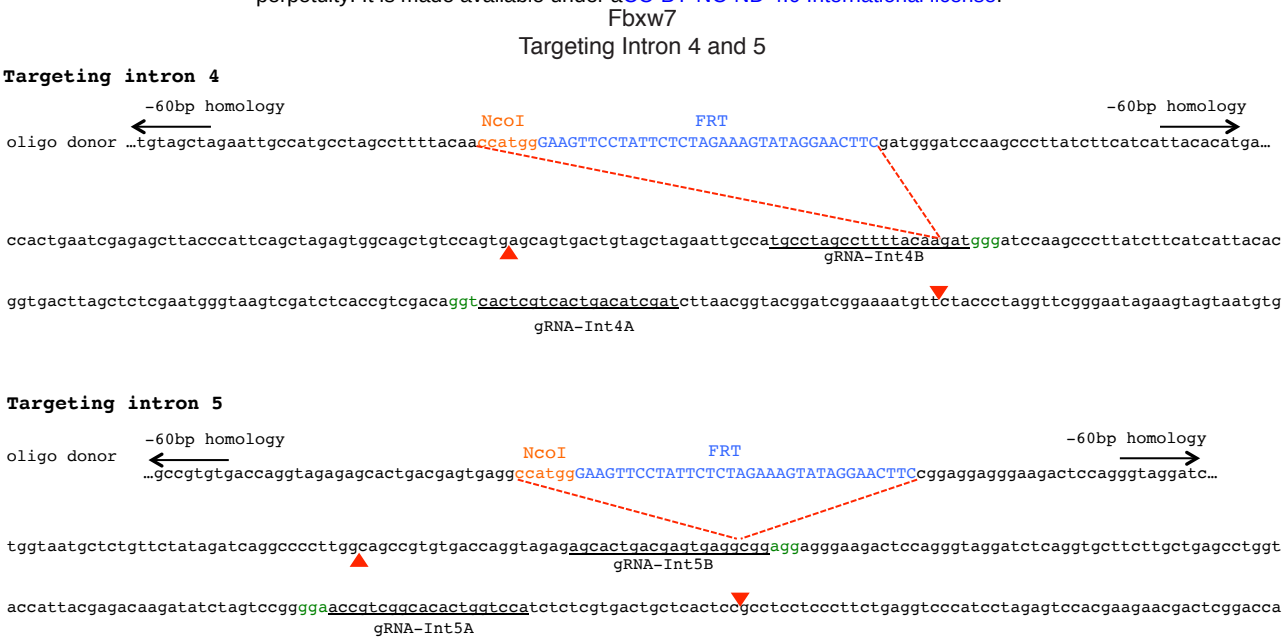

B

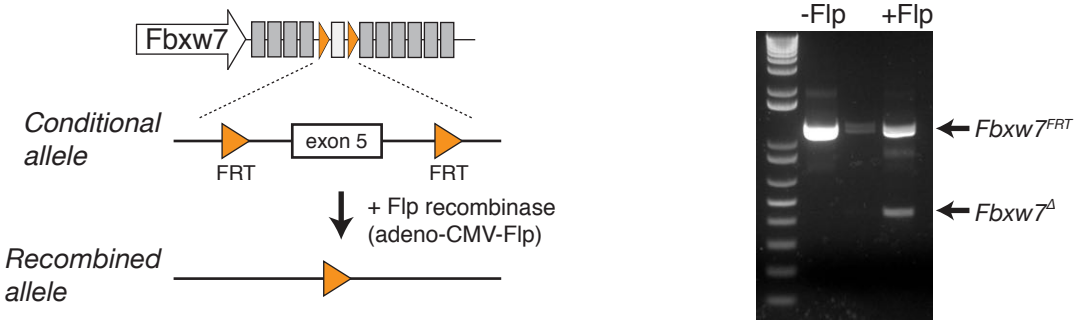

C

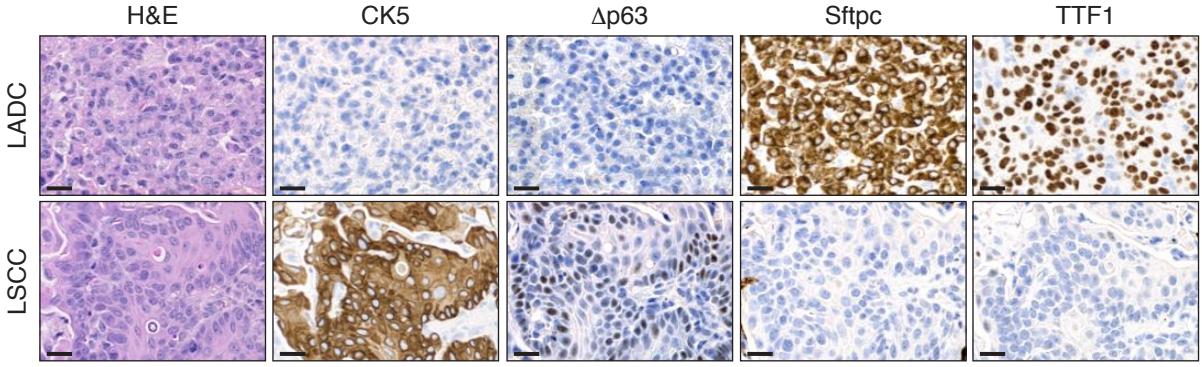

Figure S1

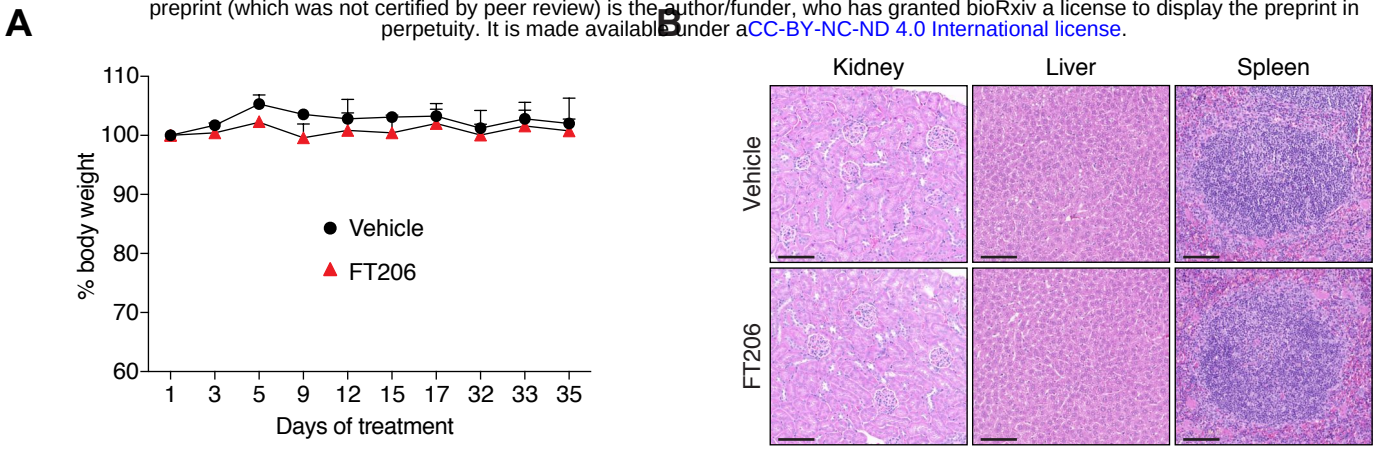

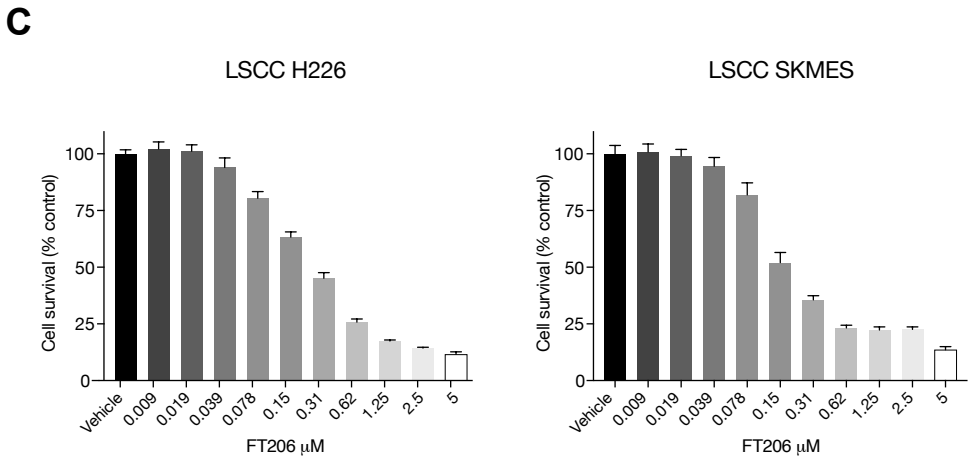

Figure S2

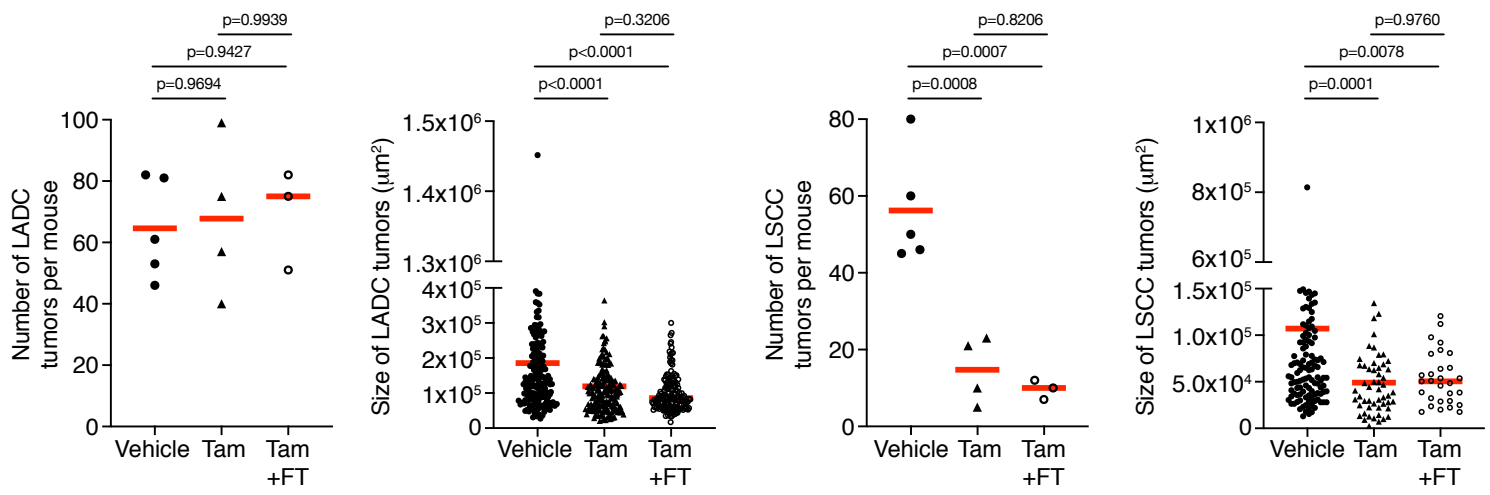

Figure S3